Acta Montanistica Slovaca
ISSN 1335-1788
actamont.tuke.sk

Deformation Characteristics and Strength Risks of Pipelines Crossing Fault Affected by Mined-out Areas

Shuren WANG[1], Ziruo WANG[2], Yuanxiu HE[3], Weibin MA[4], Xianfeng LIU[5] and Andrzej GAWLIK[6]

Authors' affiliations and addresses:
[1] School of Civil Engineering, Henan Polytechnic University, Jiaozuo 454003, China
e-mail: shurenwang@hpu.edu.cn

[2] School of Civil Engineering, Henan Polytechnic University, Jiaozuo 454003, China
e-mail: 931813862@qq.com

[3] School of Civil Engineering, Henan Polytechnic University, Jiaozuo 454003, China
e-mail: 2991817765@qq.com

[4] Railway Engineering Research Institute, China Academy of Railway Sciences Corporation Limited, Beijing 100081, China
e-mail: dwangfei@163.com

[5] Department of Road and Railway Engineering, Southwest Jiaotong University, Chengdu 610031, China
e-mail: xianfeng.liu@swjtu.edu.cn

[6] Maritime University of Szczecin, Wały Chrobrego 1-2, 70-500 Szczecin, Poland
email: a.gawlik@pm.szczecin.pl

***Correspondence:**
Shuren WANG, School of Civil Engineering, Henan Polytechnic University, Jiaozuo 454003, China
tel.: +86 15738529570
e-mail: shurenwang@hpu.edu.cn

Funding information:
Key Project of Natural Science Foundation of Henan Province, China (232300421134), First-Class Discipline Implementation of Safety Science and Engineering (AQ20230103), and Zhongyuan Science and Technology Innovation Leading Talent Program (244200510005), China.

Acknowledgement:
The authors would like to express their sincere gratitude to the editor and reviewers for their valuable comments, which have greatly improved this paper.

How to cite this article:
Wang, S., Wang, Z., He, Y., Ma, W., Liu, X. and Gawlik, A. (2025). Deformation Characteristics and Strength Risks of Pipelines Crossing Fault Affected by Mined-out Areas. *Acta Montanistica Slovaca,* Volume 30 (3), 705-715

DOI:
https://doi.org/10.46544/AMS.v30i3.12

Abstract
The buried gas pipelines crossing the mined-out areas are exposed to safety risks such as excessive deformation and stress concentration. Taking the west-east gas pipeline crossing the mined-out areas with a normal fault in China as the engineering background, a three-dimensional pipeline-soil computational model was established by using ABAQUS software. The influence factors, including fault dip angle, roof thickness of the mined-out areas, and the angle between the pipeline and fault strike on the tensile, bending, and combined tensile-bending stress response characteristics of the gas pipeline, were evaluated. Results show that increasing fault dip deepens pipeline settlement and intensifies curvature, reducing bending radius. Roof thickness changes don't alter overall deformation, but faults cause concentrated deformation. Deviation from perpendicular pipeline-fault angles raises strain, highlighting geometric control. Tensile risk K_1 is U-shaped; points 1 and 4 near yield thresholds are key tensile sites. Steeper dips and thicker roofs increase risk. Shear risk K_2 peaks at point 4, most hazardous for bending-shear. Combined stress K_3 fluctuates; point 2 is the least risky for tension, while points 1, 3, and 5 face significant bending-shear risks, needing focused protection. The conclusions obtained in this study provide a basis for assessing the safety risks of the buried gas pipelines crossing mined-out areas.

Keywords
Mined-out areas, Normal faults, Buried pipes, Tensile-bending stress, Numerical simulation, Safety risk.

Introduction

The research on long-distance buried pipelines traversing complex geological sites, particularly the mined-out areas with faults, faces numerous theoretical and technical challenges. Theoretically, while the Mohr-Coulomb model is widely used in soil behavior studies, it struggles to accurately capture nonlinear shear resistance parameters, such as internal friction angle and cohesion, of fractured rock masses in goaf areas. Conventional experiments often fail to obtain precise values for these parameters, leading to theoretical models that cannot reliably reflect actual conditions (Wang et al., 2015a; Wang et al., 2015b; Zhao et al., 2018). Technically, research on the cyclic loading characteristics of high-strength steel pipes (X80) in practical engineering remains inadequate, resulting in a lack of in-depth understanding of their long-term mechanical performance under complex geological conditions (Marino and Osouli, 2020; Rojhani et al., 2022). Additionally, real-time monitoring technologies have limitations, with a scarcity of data on early minor deformations (soil creep), which undermines the validation of prediction models built on monitoring data and makes it difficult to forecast disaster occurrences accurately.

For long-distance buried pipelines crossing the mined-out areas with fault geological conditions, several bottleneck issues exist. Experimentally, conventional methods are ineffective in measuring key parameters of fractured rock masses in mined-out areas with faults, which limits accurate assessments of geological stability. In terms of material performance, the unclear cyclic loading characteristics of high-strength steel pipes affect safety evaluations of pipelines under complex geological stresses. Monitoring-wise, difficulties in detecting early minor deformations lead to delayed disaster warnings (Farzad & Junji, 2021; Shi et al., 2024a). Furthermore, the lack of data impedes the development of precise prediction models, making it impossible to effectively forecast the evolution of disaster chains and posing significant risks to pipeline safety (Moradi et al., 2013; Gawande et al., 2019; Chen et al., 2022).

Researching long-distance buried pipelines crossing the mined-out areas with faults holds great significance. From the perspective of engineering safety, accurately obtaining parameters of fractured rock masses in the mined-out areas with faults and understanding the cyclic loading characteristics of high-strength steel pipes can optimize pipeline design and construction plans, enhance pipeline resilience in complex geological environments, and ensure the safe and stable operation of oil and gas pipelines.

State of the art

With the ongoing construction and operational expansion of China's large-scale oil and gas pipeline networks, long-distance buried pipelines increasingly traverse complex geological terrains, particularly mined-out areas intersected by faults. Research on the disaster chain involving mined-out areas, faults, and pipelines confronts multiple technical and theoretical challenges. These complex geological settings create a highly dynamic environment where the interaction between mining activities, fault movements, and pipeline integrity becomes a critical concern for ensuring the safe and reliable operation of energy infrastructure.

Previous studies by Wang et al. (2020) revealed that geological disturbances significantly govern the deformation evolution of gas pipelines under mining-induced effects. Their research emphasized that mined-out areas with faults constitute the primary factors influencing pipeline deformation. The presence of faults within or adjacent to mined-out regions exacerbates the stress redistribution in the surrounding rock mass, leading to uneven settlement and potential rupture of buried pipelines. This finding underscores the need for a more nuanced understanding of how fault-mined-out area interactions affect pipeline behavior. Qin et al. (2024) conducted a comprehensive analysis of the mechanisms underlying goaf-induced surface settlement and deformation. Their study highlighted the direct impact of mining roof thickness and extent on surface and pipeline stability. They demonstrated that thicker mining roofs and larger mined-out extents result in more pronounced surface subsidence, which in turn induces greater bending and axial stresses in buried pipelines. This research provides valuable insights into the quantitative relationship between mining parameters and pipeline deformation, offering a basis for more accurate risk assessments.

Ren et al. (2020) focused on examining the deformation and mechanical characteristics of buried pipelines in mining subsidence areas. They identified tensile and bending stresses induced by mining activities as key factors contributing to pipeline failure. Their experimental and numerical analyses revealed that pipelines crossing mined-out areas with faults experience complex stress states, including combined axial tension, bending, and shear. These findings emphasize the importance of considering multi-axial loading conditions in pipeline design and assessment. Fadaee et al. (2020) concentrated on the mechanical performance of pipelines under fault displacements, building upon earlier work by Alzabeebee (2019), Gluchowski et al. (2021), and Katebi et al. (2023). Their research explored how different fault types (normal, reverse, strike-slip) and displacement magnitudes affect pipeline integrity. They developed finite element models to simulate pipeline responses under fault movement, providing valuable data for designing pipelines resilient to seismic and tectonic activities.

Despite substantial research through experimental and numerical methods on buried pipelines traversing mined-out areas with faults (Nair et al., 2024; Liu et al., 2024; Jalali et al., 2024), risk analysis regarding pipeline

deformation and strength remains insufficient (Phan et al., 2023; Shi et al., 2024b; Battistelli et al., 2025). Current methodologies often fail to account for the cumulative effects of mining-induced subsidence and fault movements over the pipeline's service life. Moreover, there is a lack of standardized protocols for assessing the long-term performance of pipelines in these complex environments. Addressing these gaps requires integrated approaches that combine advanced monitoring technologies, improved numerical modeling, and probabilistic risk assessment methods to ensure the safety and reliability of China's critical energy infrastructure.

Based on the west-east gas pipeline crossing a normal fault in the mine-out areas in Henan Province, China, the pipeline response characteristics were analyzed under special geological conditions by using numerical simulations (Emre et al., 2021; Darvishi et al., 2024). The pipeline failure mechanisms under multi-factor coupling effects were investigated, and a risk coefficient-based safety evaluation system was established, which provided references for designing and optimizing long-distance pipelines and mitigating risks in similar complex geological settings. Additionally, identifying and analyzing key monitoring points offers scientific guidance for pipeline monitoring layouts, significantly enhancing the safety and reliability of pipeline engineering.

Methodology

Building a computational model

Taking the west-east gas pipeline crossing a normal fault in the mine-out areas in China as the engineering background, a three-dimensional numerical model was constructed. Given the vast scale of soil mass and the considerable axial length of the pipeline, coupled with the need to account for fault impacts and pipe-soil interactions, the finite element analysis demands careful consideration of the region experiencing significant deformation near the fault. For this zone, the selected pipeline length should be no less than 60 times the pipeline diameter to facilitate an accurate study. In this study, a pipeline with an outer diameter of D was modeled over a length of 80D, while the overall fault soil model dimensions were set at 80D, 40D, and 30D along the *x*-, *y*-, and *z*- axes, respectively. The constructed buried pipeline model, set in mine-out zones intersected by a fault, accurately simulates the relative downward movement of the hanging wall, while also integrating the process of ground subsidence. Based on an analysis of the mine-out areas in the Henan section of the west-east gas pipeline, the mine-out areas were positioned on the hanging wall, as illustrated in Fig. 1.

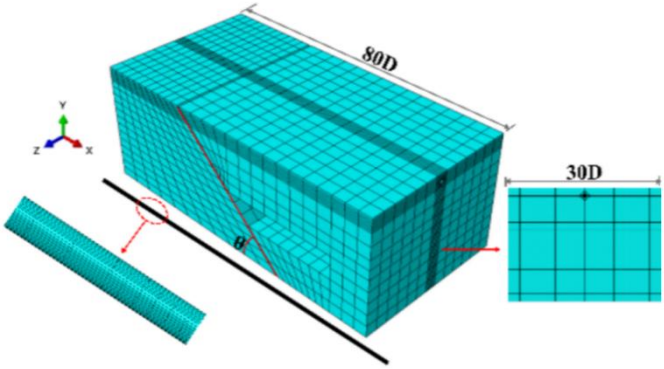

Fig. 1. Computational model of buried pipeline-soil system

Calculation parameters and constitutive relations

In Abaqus, the interaction settings between the pipeline and soil primarily consist of two components: normal interaction and tangential interaction. The normal interaction is configured as a hard contact, enabling the transfer of normal pressure between the pipeline and soil. Additionally, this setting allows for separation between the pipeline and soil upon contact. The tangential interaction is set as a penalty friction model, which accounts for the frictional forces between the pipeline and soil.

For this study, an X80 pipeline is selected, a commonly used pipe material in the west-east gas pipeline project in China. The pipeline is modeled using an elastic-plastic stress-strain constitutive relation for X80 steel to simulate plastic deformation induced by fault actions. The stress-strain relationship is described by the following equation:

$$\varepsilon = \frac{\sigma_s}{E}\left[\frac{\sigma}{\sigma_s} + \lambda\left(\frac{\sigma}{\sigma_s}\right)^N\right] \tag{1}$$

where ε represents the total strain, σ represents the stress, σ_s is the yield stress, taken as 552 MPa, E is the initial elastic modulus, taken as 210 GPa, λ and N are dimensionless parameters, taken as 0.981 and 19.12, respectively.

The real stress-strain fitting curve of the X80 pipe is shown in Fig. 2.

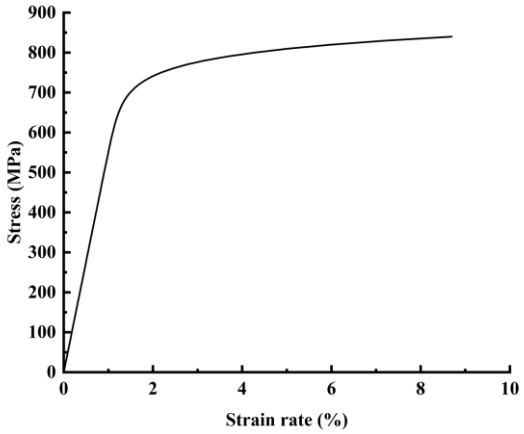

Fig. 2. Real stress-strain curve of X80 pipeline

The soil is modeled using the Mohr-Coulomb constitutive model, which incorporates Hooke's Law for elastic behavior and Coulomb's failure criterion. Physical and mechanical properties of the soil, such as strain softening, are simulated by setting parameters including the internal friction angle, cohesion, and dilation angle. The friction coefficient between the pipeline and soil is selected as 0.3. Relevant parameters for the computational model are listed in Table 1.

Tab. 1. Calculation parameters of the model

Name	Density (kg/m^3)	Elastic modulus (MPa)	Poisson's ratio	Internal friction angle (°)	Cohesion (kPa)	Dilation angle (°)
Topsoil	1930	20	0.35	18	45	0.1
Weathered sandstone	2450	16000	0.30	28	2700	8
Coal seam	1380	5000	0.32	21	1200	7
Sandstone	2650	24000	0.25	38	6000	12

Boundary conditions

The entire soil model is considered as a hexahedron. Under initial conditions, no constraints are applied to the top surface. At the bottom of the soil model, displacements in the *x*-, *y*-, and *z*- directions are constrained, while rotational constraints are not applied. For the four lateral sides of the soil model, displacements in the normal direction are constrained. During the numerical simulation, a small relative sliding occurs between the pipeline and the soil. Therefore, spring loads are applied to the pipeline end on the fixed side. It should be noted that the bottom of the pipe-soil model in this study does not extend to the bedrock surface. Consequently, the applied displacements represent surface dislocations of the upper soil layers caused by bedrock fracture dislocations in the lower overburden, rather than bedrock dislocations themselves. The primary loads considered include gravity, internal pressure on the pipeline's inner surface, and fault displacement loads.

The entire analysis process is divided into four sequential steps: First, the gravity is applied to the entire model. Second, a uniformly distributed load pressure is applied to the inner surface of the pipeline. Third, while keeping the lower plate stationary, constraints on the upper plate are removed, and a linear displacement load is applied to simulate relative motion between the two fault blocks. Fourth, the overburden soil above the mined-out areas is allowed to collapse downward. All four analysis steps employ a general static analysis procedure.

Simulation conditions

Influence of fault angle on pipeline: To investigate the effect of fault angle on the pipeline, the following model parameters are selected: pipeline burial depth of 2.0 m, outer diameter of 1219 mm, and wall thickness of 22 mm. The constitutive model parameters for the soil remain consistent with those described earlier to ensure result comparability. The internal pressure is set at 10 MPa, while the magnitude of fault displacement and the degree of roof (referring to the weathered sandstone layer in the upper plate, henceforth not repeated) collapse remain constant. The weathered sandstone thickness is 5 m, and the angle between the pipeline and fault strike is maintained at 90° to ensure uniformity in variable control. Three typical fault angles -45°, 50°, and 55° are analyzed with an interval of 5° to study the impact of angle variation on the pipeline's structural response.

Influence of roof thickness on pipeline: To explore the effect of roof thickness in the mined-out areas on the pipeline, the pipeline burial depth is set at 2.0 m, with an outer diameter of 1219 mm and a wall thickness of 22 mm. The internal pressure is 10 MPa, the fault angle is 45°, and the magnitudes of fault displacement and roof

collapse remain unchanged. The angle between the pipeline and fault strike is maintained at 90° for consistent variable control. Three roof thicknesses -3 m, 4 m, and 5 m are analyzed with a distance interval of 1 m to investigate their impact on the pipeline.

Influence of pipeline-fault strike angle on pipeline: To assess the effect of the angle between the pipeline and fault strike on the pipeline, the pipeline has an outer diameter of 1219 mm and a wall thickness of 22 mm. The internal pressure is 10 MPa, the magnitudes of fault displacement and roof collapse remain constant, and the roof thickness in the mined-out areas is 5 m. Three angles between the pipeline and fault strike -80°, 85°, and 90° are analyzed with an interval of 5° to study their impact on the pipeline.

Results analysis and discussion

Analysis of pipeline deformation characteristics affected by the fault

Influence of fault dip angle on pipeline deformation: The numerical simulation results reveal the pipeline deformation trends under three different fault angles, as illustrated in Fig. 3. As the fault dip angle increases, the location of significant strain in the *y*-direction shifts positively along the *x*-axis. This occurs because variations in fault angle alter the contact angle and position between the fault plane and the pipeline, causing the location of large deformations to change accordingly. Specifically, as the fault dip angle progresses from 45° to 50° and then to 55°, the magnitude of subsidence increases sequentially. The trough becomes deeper and shifts slightly backward, while the slope of the recovery section steepens. This indicates a reduction in bending radius and an intensification of curvature concentration.

Influence of roof thickness on pipeline deformation: The numerical simulation results indicate that buried pipelines under different roof thicknesses in the mined-out areas exhibit significant deformation at the fault plane and collapse zones, as shown in Fig. 4 . Notably, as the roof thickness increases, the overall deformation trend of the pipeline remains largely consistent without substantial differences.

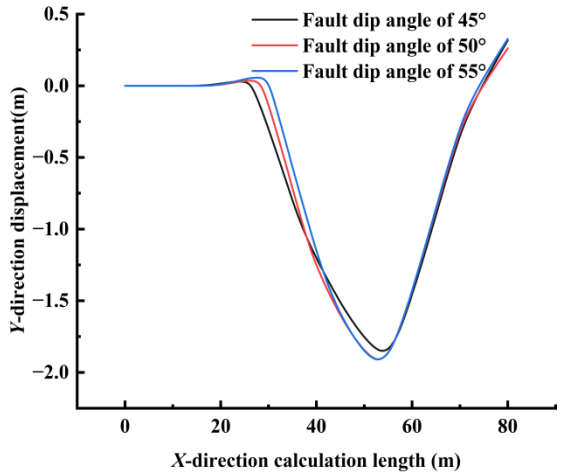

Fig. 3. Influence of fault angle on pipeline deformation

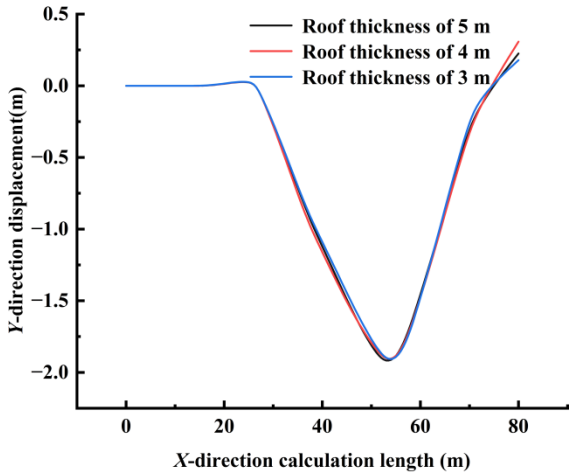

Fig. 4. Influence of the roof thickness on pipeline deformation

Influence of the angle between pipeline and fault strike on pipeline deformation: The numerical simulation results, as illustrated in Fig. 5, reveal that under all three angles, pipeline displacement exhibits a similar pattern: rapid subsidence upon entering the fault zone, forming a trough at approximately 50 m, followed by recovery. The trough depth varies with the angle: it is greatest at 80°, intermediate at 85°, and smallest at 90°. Notably, the recovery rate is fastest at 90°, with more pronounced uplift observed at the end section (70-80 m). The pipeline deformation characteristics across the three angles are similar to those observed in the previous two cases. Specifically, when the angle between the pipeline and fault plane is 90°, the strain experienced by the pipeline is minimized.

Analysis of the tensile strength risk of a pipeline affected by the fault

When selecting pipeline strength monitoring points, five key positions were determined based on the common deformation features and the distribution of equivalent stress (Mises stress) extrema. Taking the influence of different pipeline-fault angles on deformation as an example, the five points are located at 1 m, 7.5 m, 12 m, 31 m, and 45 m along the *x*-axis from the starting point of the fault-fracture zone (Figs. 6 and 7). All subsequent data are obtained from these five points.

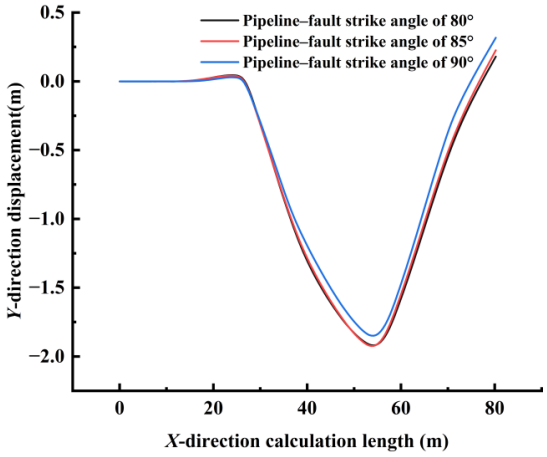

Fig. 5. Influence of the angle between the pipeline and the fault direction on the pipeline deformation

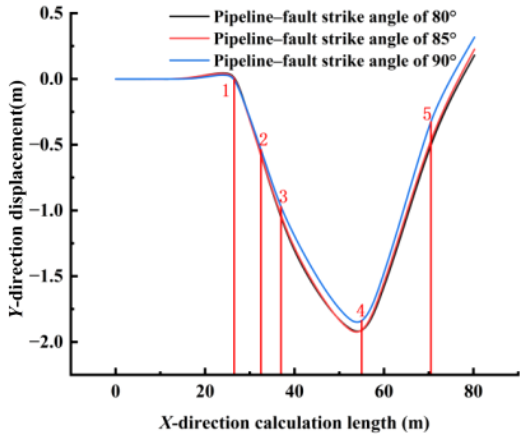

Fig. 6. Five monitoring points of the pipeline deformation

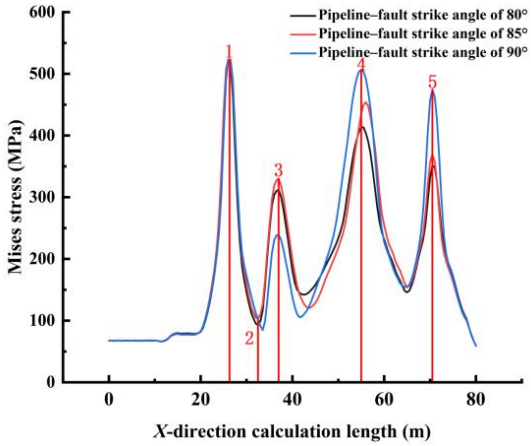

Fig. 7. Five monitoring points of the pipeline Mises stress

Due to the complex stress conditions affecting buried pipeline deformation under various operational scenarios, the tensile strength risk coefficient K_1 is defined as the ratio of the tensile stress experienced by the pipeline to the yield stress of the pipeline material. Mathematically, K_1 is expressed as:

$$K_1 = \frac{\sigma}{\sigma_y} \tag{2}$$

where σ represents the axial tensile stress, σ_y is the yield stress of the pipeline material, taken as 552 MPa.

This coefficient quantifies the proportion of tensile stress relative to the material's yield limit, providing an intuitive measure of the potential risk for tensile failure in the pipeline under applied loads. A ratio closer to 1 indicates that the tensile stress is nearing the material's yield threshold, thereby increasing the risk of tensile failure in the pipeline.

Influence of fault dip angle on tensile strength risk of pipeline: The tensile risk coefficients K_1 for pipelines under different fault dip angles were calculated as illustrated in Fig. 8. The K_1 values exhibit an overall U-shaped variation across different fault dip angles, with the lowest value observed at Point 2, followed by a gradual increase. Points 1 and 4 are closest to 1, indicating the highest risk of tensile failure at these locations. As the fault dip angle progresses from 45° to 50° and then to 55°, the curve shifts upward overall. At 55°, the K_1 values for all measurement points are closer to 1, suggesting that the pipeline's tensile state is nearing the yield threshold, thereby significantly increasing the risk of failure. Conversely, the 45° fault dip angle presents the lowest risk. These findings indicate that as the fault dip angle increases, the risk of tensile failure in the pipeline also rises.

Influence of roof thickness on tensile strength risk of pipeline: The tensile risk coefficients K_1 for pipelines under different roof thicknesses were calculated as shown in Fig. 9. K_1 reaches its lowest value at Point 2 and then gradually increases, stabilizing at Points 4 and 5. Under varying roof thicknesses, a thicker roof generally corresponds to a higher overall K_1 level, indicating that the tensile stress in the pipeline is closer to the yield threshold, thereby increasing the risk of failure. Specifically, when the roof thickness is 5 m, the curve is highest overall, signifying the lowest level of safety. These findings demonstrate that roof thickness has a significant impact on the tensile performance of the pipeline, with an increase in roof thickness exacerbating tensile stress concentration in the rear section of the fault zone.

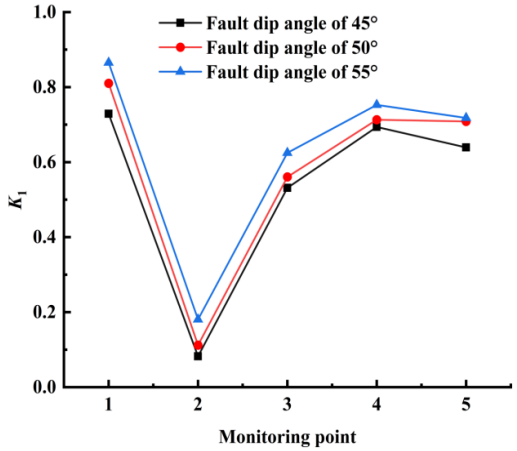

Fig. 8. Risk coefficient curves under different fault dip angles

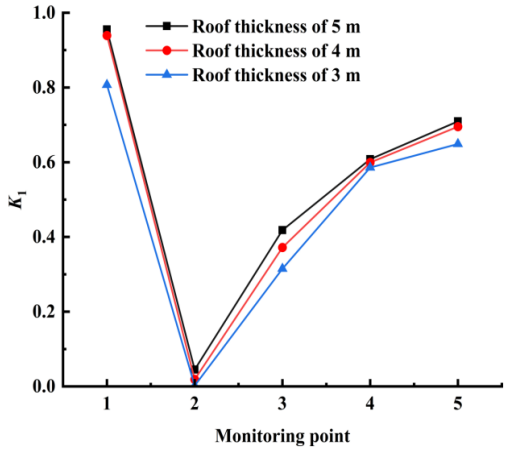

Fig. 9. Risk coefficient curves under different roof thicknesses

Influence of angle between pipeline and fault strike on tensile strength risk of pipeline: As shown in Fig. 10, the tensile risk coefficients K_1 for pipelines under different angles between the pipeline and fault strike were determined. Along the pipeline, K_1 exhibits a pattern of initial decrease-rapid and increase-post-peak decline: it is lowest at Point 2, peaks at Point 4, and slightly decreases at Point 5. The curve is highest overall for an 80° angle, followed by 85°, and lowest for 90°. This indicates that a smaller angle brings the tensile stress closer to the yield threshold, thereby increasing the risk of tensile failure.

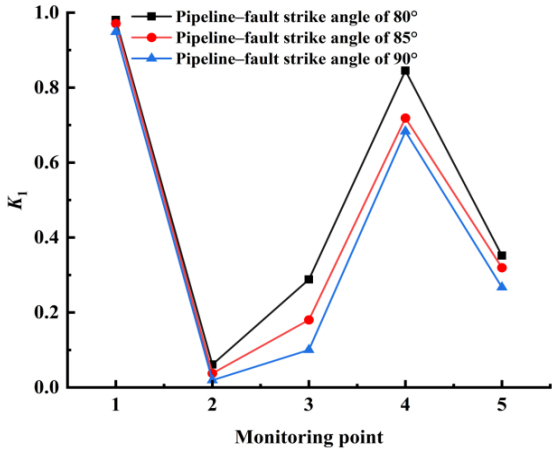

Fig. 10. Tensile strength risk coefficient curves at five points along the pipeline under different angles

Analysis of the bending strength risk of a pipeline affected by the fault

Due to the complex stress conditions acting on buried pipelines during deformation under various operational scenarios, the bending strength risk coefficient K_2 is defined as the ratio of the shear stress experienced by the pipeline to the yield stress of the pipeline material.

$$K_2 = \frac{\tau}{\tau_y} \tag{3}$$

where, K_2 represents the bending strength risk coefficient. τ denotes the shear stress. τ_y is the yield stress of the pipeline material.

This coefficient K_2 quantifies the proportion of shear stress relative to the material's yield limit, providing an intuitive measure of the potential risk for bending-shear failure in the pipeline under applied loads. A ratio closer to 0.577 (which corresponds to the shear yield criterion for some materials, representing the point where shear stress reaches a critical level relative to uniaxial yield stress) indicates that the shear stress is nearing the material's yield threshold, thereby increasing the risk of bending-shear failure in the pipeline.

Influence of fault dip angle on bending strength risk of pipeline: As shown in Fig. 11, the bending strength risk coefficient K_2 along the pipeline exhibits a trend of gradual increase-sharp rise-postpeak decline, with Point 4 reaching the peak value. As the fault dip angle increases from 45° to 50° and then to 55°, the overall curve shifts upward. Using 0.577 as the yield threshold criterion: at Point 4, the 50° angle comes closest to this threshold, indicating the highest risk of bending-shear failure. Although the 55° angle shows higher numerical values, it deviates further from the threshold, resulting in a relatively lower risk.

Influence of roof thickness on bending strength risk of pipeline: As shown in Fig. 12, the bending strength risk coefficient K_2 along the pipeline exhibits a trend of decline → rise → peak → decline, with Point 2 at the lowest value and Point 4 at the peak. As the roof thickness decreases from 5 m to 4 m and then to 3 m, the overall curve shifts upward. At a roof thickness of 3 m, the K_2 value at Point 4 is closest to the 0.577 threshold, indicating the highest risk of bending-shear failure. Conversely, when the roof thickness is 5 m, the overall K_2 values are the lowest, representing the best safety performance.

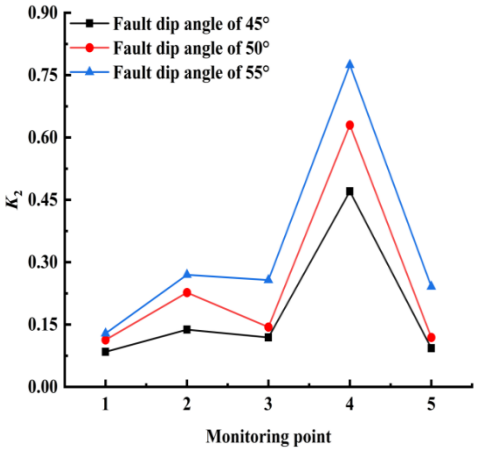

Fig. 11. Risk coefficient curves under different angles

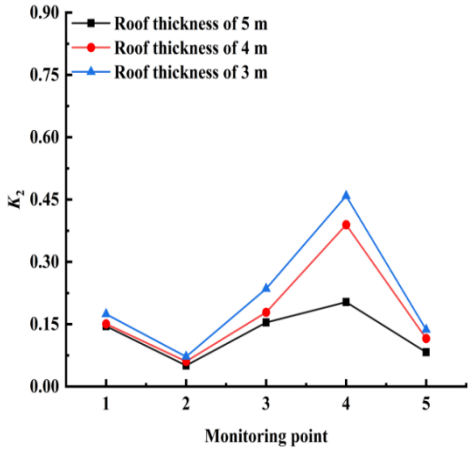

Fig. 12. Risk coefficient curves under different thicknesses

Influence of angle between pipeline and fault strike on bending strength risk of pipeline: As shown in Fig. 13, the bending strength risk coefficient K_2 along the pipeline initially decreases gradually to its lowest point at Point 3, then rises sharply to form a peak at Point 4, before declining again at Point 5. As the angle between the pipeline and fault strike approaches perpendicularity (from 80° to 85° and then to 90°), the overall curve shifts upward, with Point 4 getting progressively closer to the 0.577 threshold. This indicates a higher risk of bending-shear failure, with the most significant differences observed at Point 4: the 90° angle poses the greatest risk of bending-shear failure; the 85° angle follows; and the 80° angle is relatively safer.

Analysis of tensile-bending coupling strength risk of pipelines affected by the fault

The tensile-bending coupling strength risk coefficient K_3 is defined as the ratio of the bending strength risk coefficient K_2 to the tensile strength risk coefficient K_1; it experiences:

$$K_3 = \frac{K_2}{K_1} \tag{4}$$

This coefficient K_3 quantifies the proportion of shear stress relative to tensile stress, providing an intuitive measure of the potential risk for combined bending-shear and tensile failure in the pipeline under applied loads. When the ratio is less than 1, it indicates a higher risk of tensile failure in the pipeline. Conversely, when the ratio exceeds 1, the risk of bending-shear failure becomes more prominent.

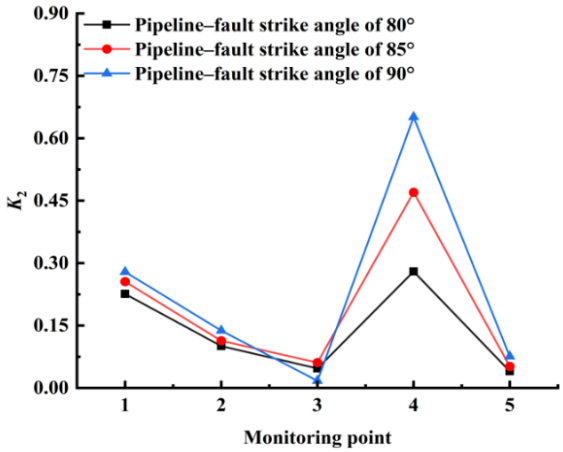

Fig. 13. Curves of bending strength risk coefficient at five points of the pipeline under different angles

Influence of fault dip angle on tensile-bending coupling strength risk of pipeline: As shown in Fig. 14, the tensile-bending coupling strength risk coefficient K_3 exhibits a trend of decline-slight recovery-minor decline-subsequent rise along the pipeline, with the minimum value occurring at Point 2, approaching zero. As the fault dip angle increases from 45° to 50° and then to 55°, the overall curve shifts downward. At a dip angle of 55°, Points 3 to 5 are closer to or even approach a value of 1, indicating a tendency toward tensile failure. In contrast, under a 45° dip angle, Points 1, 3, and 5 show significantly higher values (>1), suggesting a more pronounced dominance of bending-shear failure.

Influence of roof thickness on tensile-bending coupling strength risk of pipeline: As shown in Fig. 15, the K_3 curve exhibits a steep decline-gentle rise pattern along the pipeline, with Point 2 representing the minimum trough value. As the roof thickness decreases from 5 m to 4 m and then to 3 m, the overall K_3 values across the pipeline shift downward. Under a 3 m roof thickness scenario, K_3 falls below 1 at multiple locations between Point 1 and Point 3, indicating that tensile failure becomes the dominant failure mode. Conversely, under a 5 m roof thickness, K_3 exceeds 1 at several points, suggesting that bending-shear failure is more controlling. The 4 m roof thickness represents an intermediate condition between these two extremes.

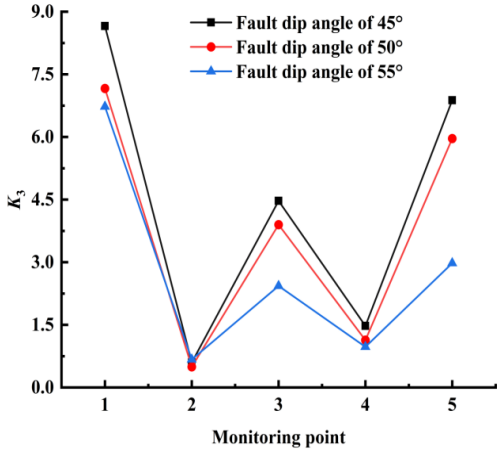

Fig. 14. Risk coefficient curves under different angles

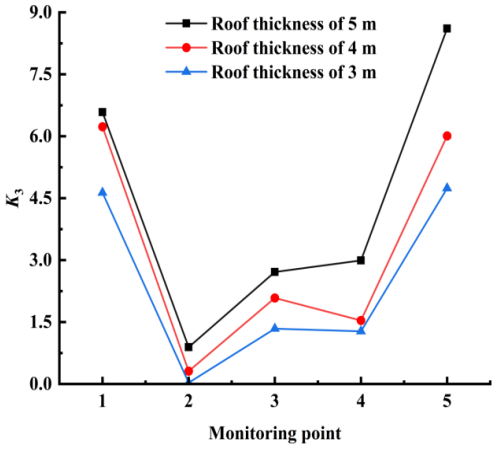

Fig. 15. Risk coefficient curves under different roof thicknesses

Influence of angle between pipeline and fault strike on tensile-bending strength risk of pipeline: As shown in Fig. 16, the K_3 curve exhibits an overall fluctuating trend: Point 2 represents the lowest trough, Point 3 shows a notable increase, and Point 5 reaches another peak. As the angle between the pipeline and fault strike increases from 80° to 85° and then to 90°, the entire curve gradually shifts downward. This indicates that a larger angle results in a smaller K_3 value, with the pipeline tending more toward tensile failure. Conversely, at smaller angles, K_3 values generally exceed 1, indicating that bending-shear effects dominate. It is evident that under a 90° angle, the pipeline is more prone to tensile failure risks.

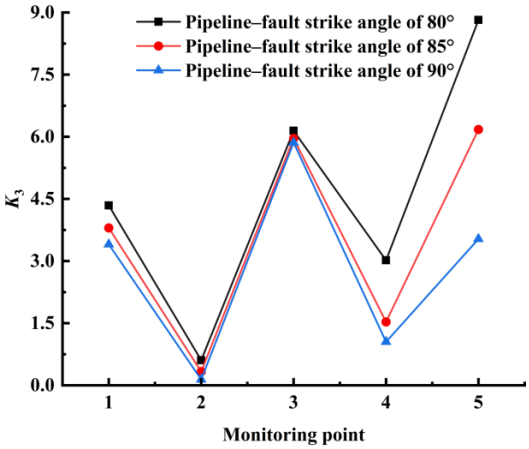

Fig. 16. Risk coefficient curves of tensile-bending coupling strength at five points of the pipeline under different angles

Conclusions

Using finite element software ABAQUS, this study investigates the mechanical response of X80 buried pipelines under the mined-out areas with a normal fault, based on the background of the west-east gas pipeline

project. The research primarily considers three influencing factors: fault dip angle, roof thickness, and the angle between the pipeline and fault strike. A risk coefficient is employed to evaluate the pipeline's susceptibility to failure under different scenarios. The main conclusions are obtained as follows:

(1) Increasing fault dip deepens pipeline settlement troughs and intensifies curvature concentration, reducing bending radius. Roof thickness variations in the mined-out areas don't alter overall deformation trends, but concentrated deformation occurs at faults and subsidence zones, indicating limited roof control. The angle between the pipeline and fault significantly affects trough depth and recovery rate; greater deviation from perpendicularity (90°) increases strain and deformation, highlighting geometric matching as the dominant factor.

(2) Tensile stress risk coefficient K_1 follows a U-shaped distribution, with monitoring point 2 at the lowest risk and points 1 and 4 nearing yield thresholds, making them key tensile failure control sites. Larger fault dips and thicker roofs elevate overall risk, pushing the pipeline closer to yielding. Smaller pipeline-fault angles significantly raise tensile risk, making points 1 and 4 the most tensile-sensitive. Shear stress risk coefficient K_2 peaks at point 4, closest to the 0.577 critical value, marking it as the most hazardous bending-shear location. Risks rise with steeper fault dips, thinner roofs, and more perpendicular angles, especially at a 90° angle, 3 m roof thickness, and 50° fault dip, where point 4's bending-shear risk is prominent.

(3) Combined tensile-shear stress risk coefficient K_3 fluctuates, with point 2 at the lowest risk, indicating strong tensile fracture control. Points 1, 3, and 5 show higher values under varying conditions, reflecting enhanced bending-shear effects. Steeper fault dips or thinner roofs generally lower K_3, emphasizing tensile fracture dominance. Smaller pipeline-fault angles often push K_3 above 1, indicating stronger bending-shear effects. Overall, point 2 is the primary tensile risk site under combined stress, while points 1, 3, and 5 also face significant bending-shear risks, requiring focused protection.

Given that this study did not fully account for complex effects such as soil nonlinearity, creep, and cyclic loading, the pipeline response under long-term service conditions still requires further investigation. Additionally, there is a lack of systematic validation of the simulation results through field measurements or experimental data. Subsequent research will integrate on-site monitoring data with numerical simulations for mutual verification, incorporate multi-field coupling and stochastic analysis, and further refine the risk coefficient evaluation system. The aim is to provide a more universal and reliable safety assessment methodology for the pipeline crossing the mined-out areas.

Reference

Alzabeebee, S. (2019). Seismic response and design of buried concrete pipes subjected to soil loads. Tunnelling and Underground Space Technology, 93, pp. 103084. DOI: 10.1016/j.tust.2019.103084.

Battistelli, M., Ferrarini, F., Bucci, F., Santangelo, M., Cardinali, M., Boncori, J. P. M., Cirillo, D., Carafa, M. M. C. (2025). Bridging the gap between active faulting and deformation across normal-fault Systems in the central-southern apennines (Italy): multi-scale and multi-source data analysis. Remote Sensing, 17(14), pp. 2491. DOI: 10.3390/rs17142491.

Chen, Y. F., Hou, F. H., Dong, S. H., Guo, L. Y., Xia, T. J., He, G. Y. (2022). Reliability evaluation of corroded pipeline under combined loadings based on back propagation neural network method. Ocean Engineering, 262, pp. 111910. DOI: 10.1016/j.oceaneng.2022.111910.

Darvishi, R., Jafarian, Y., Lashgari, A., Askari, F. (2024). Seismic interactive deformations of pipeline buried in sandy slopes using numerical modeling with a systematic calibration procedure. Journal of Pipeline Systems Engineering and Practice, 15(3), pp. 04024029. DOI: 10.1061/JPSEA2.PSENG-1567.

Emre, H. D., Mustafa, K., Subhamoy, B. (2021). Behaviour of buried continuous pipelines crossing strike-slip faults: Experimental and numerical study. Journal of Natural Gas Science and Engineering, 92, pp. 103980. DOI: 10.1016/j.jngse.2021.103980.

Fadaee, M., Farzaneganpour, F., Anastasopoulos, I. (2020). Response of buried pipeline subjected to reverse faulting. Soil Dynamics and Earthquake Engineering, 132, pp. 106090. DOI: 10.1016/j.soildyn.2020.106090.

Farzad, T., Junji, K. (2021). A refined nonlinear analytical method for buried pipelines crossing strike‐slip faults. Earthquake Engineering & Structural Dynamics, 50(11), pp. 2915-2938. DOI: 10.1002/eqe.3479.

Gawande, K., Kiran, R., Cherukuri, H. P. (2019). A numerical study of the response of buried steel pipelines undergoing strike-slip fault. Engineering Failure Analysis, 102, pp. 203-218. DOI: 10.1016/j.engfailanal.2019.04.026.

Gluchowski, A., Sadzevicius, R., Skominas, R., Sas, W. (2021). Compacted anthropogenic materials as backfill for buried pipes. Materials, 14(4), pp. 717, DOI: 10.3390/ma14040717.

Jalali, H., Khaksar, R. Y., Mohammadzadeh, S. D., Karballaeezadeh, N., Gandomi, A. H. (2024). Prediction of vertical displacement for a buried pipeline subjected to normal fault using a hybrid FEM-ANN approach. Frontiers of Structural and Civil Engineering, 18(3), pp. 428-443. DOI: 10.1007/s11709-024-1015-0.

Liu, P. F., Wang, W. Y., Xu, G. Y., Wang, S. R., He, Y. X. (2024). Identification method of high consequence area of pipeline based on deep learning and GIS technology. Journal of Engineering Science and Technology Review, 17(6), pp. 216-223. DOI: 10.25103/jestr.176.24.

Marino, G., Osouli, A. (2020). Slip resistance behavior of coal tar-coated steel pipelines buried in clayey and sandy backfills from ground movement. Journal of Pipeline Systems Engineering and Practice, 11(3), pp. 05020001. DOI: 10.1061/(ASCE)PS.1949-1204.0000465.

Moradi, M. Rojhani, M., Galandarzadeh, A., Takada, S. (2013). Centrifuge modeling of buried continuous pipelines subjected to normal faulting. Earthquake Engineering and Engineering Vibration, 12(1), pp. 155-164. DOI: 10.1007/s11803-013-0159-z Published MAR 2013.

Nair, G. S., Dash, S. R., Mondal, G. (2024). Response of horizontally bent buried pipelines subjected to strike-slip faulting: a numerical investigation. Journal of Pipeline Systems Engineering and Practice, 15(3), pp. 04024031. DOI: 10.1061/JPSEA2.PSENG-1480.

Katebi, M., Wijewickreme, D., Maghoul, P., Roy, K. (2023). Lateral force-displacement response of buried pipes in slopes. Geotechnique, 73(5), pp. 375-387. DOI: 10.1680/jgeot.21.00057.

Phan, H. C., Dhar, A. S., Bui, N. D. (2023). Reliability assessment of pipelines crossing strike-slip faults considering modeling uncertainties using ANN models. Reliability Engineering and System Safety, 237, pp. 109371. DOI: 10.1016/j.ress.2023.109371.

Qin, M., Bai, J. K., Song, Y., Lv, G. Y., He, H. S. (2024). Multidimensional analysis and research on the impact of goaf on the surface. China Mining Magazine, 33(9), pp. 80-87. DOI: 10.12075/j.issn.1004-4051.20220909

Ren, J, D., Wang, W., Dong, M., Gao, S, S. (2020). Analysis of deformation and mechanical characteristics of buried pipelines in mining subsidence areas. China Safety Science Journal, 30(10), pp. 82-89. DOI: 10.16265/j.cnki.issn1003-3033.2020.10.012.

Rojhani, M., Moradi, M., Derakhshani, A. (2022). Innovative mitigation method for buried pipelines crossing faults. Earthquake Engineering and Engineering Vibration, 21(4), pp. 1089-1101. DOI: 10.1007/s11803-022-2122-3.

Shi, K. P., Wang, S. R., Liu, X. F., Ma, W. B., Chang, Y. G. (2024a). Surface movement and stability analysis of buildings above mined-out areas. Journal of Engineering Science and Technology Review, 17(3), pp. 228-234. DOI:10.25103/jestr.173.23.

Shi, K. P., Wang, S. R., Ma, W. B., Chen, W. X., Rabe, M. (2024b). Dynamic response characteristics of foundation of mined-out areas under high-speed railway load. Acta Montanistica Slovaca, 29(1), pp. 26-38. DOI: 10.46544/AMS.v29i1.03.

Wang, S. R., Li, N., Li, C. L., Cao, C. (2015a). Distribution characteristics analysis of the pressure-arch in horizontal stratified rocks under coal mining. Tehnicki Vjesnik-Technical Gazette, 22(4), pp. 997-1004. DOI: 10.17559/TV-20141207160855.

Wang, S. R., Li, N., Li, C. L., Zou, Z. S., Chang, X. (2015b). Instability mechanism analysis of pressure-arch in coal mining field under different seam dip angles. DYNA, 90(3), pp. 279-284. DOI: 10.6036/7530.

Wang, W., Ren, J, D., Dong, M., Zhang, S. W., Sun, H. (2020). A simulation experimental study on deformation evolution of natural gas pipeline under mining influence. Journal of Mining & Safety Engineering, 37(4), pp. 777-787. DOI: 10.13545/j.cnki.jmse.2020.04.016.

Zhao, Y. H., Wang, S. R., Zou, Z. S., Ge, L. L., Cui, F. (2018). Instability characteristics of the cracked roof rock beam under shallow mining conditions. International Journal of Mining Science and Technology, 28(3), pp. 437-444. DOI: 10.1016/j.ijmst.2018.03.005.